

# Experimental evidence for $^{56}\text{Ni}$ -core breaking from the low-spin structure of the $N = Z$ nucleus $^{58}_{29}\text{Cu}_{29}$

A.F. Lisetskiy,<sup>1,2</sup> N. Pietralla,<sup>1</sup> M. Honma,<sup>3</sup> A. Schmidt,<sup>1</sup> I. Schneider,<sup>1</sup>  
A. Gade,<sup>1,2</sup> P. von Brentano,<sup>1</sup> T. Otsuka,<sup>4</sup> T. Mizusaki,<sup>5</sup> and B. A. Brown<sup>2</sup>

<sup>1</sup> *Institut für Kernphysik, Universität zu Köln, 50937 Köln, Germany*

<sup>2</sup> *National Superconducting Cyclotron Laboratory,*

*Michigan State University, East Lansing, Michigan 48824-1321*

<sup>3</sup> *Center for Mathematical Sciences, University of Aizu, Tsuruga,  
Ikki-machi, Aizu-Wakamatsu, Fukushima 965-8580, Japan*

<sup>4</sup> *Department of Physics and Center for Nuclear Studies,  
University of Tokyo, Hongo, Tokyo 113-033, Japan and RIKEN,*

*Horosawa, Wako-shi, Saitama 351-0198, Japan and*

<sup>5</sup> *Institute of Natural Sciences, Senshu University,  
Higashimita, Tama, Kawasaki, Kanagawa 214-8580, Japan*

(Dated: July 10, 2018)

Low-spin states in the odd-odd  $N = Z$  nucleus  $^{58}\text{Cu}$  were investigated with the  $^{58}\text{Ni}(p,n\gamma)^{58}\text{Cu}$  fusion evaporation reaction at the FN-TANDEM accelerator in Cologne.  $\gamma\gamma$ -coincidences,  $\gamma\gamma$ -angular correlations, and signs of  $\gamma$ -ray polarizations were measured. Seventeen low spin states below 3.6 MeV and 17 new transitions were observed. Ten multipole mixing ratios and 17  $\gamma$ -branching ratios were determined for the first time. New detailed spectroscopic information on the  $2_2^+$  state, the Isobaric Analogue State (IAS) of the  $2_1^+, T = 1$  state of  $^{58}\text{Ni}$ , makes  $^{58}\text{Cu}$  the heaviest odd-odd  $N = Z$  nucleus with known  $B(E2; 2_2^+, T = 1 \rightarrow 0^+, T = 1)$  value. The  $4^+$  state at 2.751 MeV, observed here for the first time, is identified as the IAS of the  $4_1^+, T = 1$  state in  $^{58}\text{Ni}$ . The new data are compared to full  $pf$ -shell model calculations with the novel GXPF1 residual interaction and to calculations within a  $pf_{5/2}$  configurational space with a residual surface delta interaction. The role of the  $^{56}\text{Ni}$  core excitations for the low-spin structure in  $^{58}\text{Cu}$  is discussed.

PACS numbers: 21.10.Hw, 21.60.Cs, 23.20.Lv, 27.40.+z

## I. INTRODUCTION

Odd-odd  $N = Z$  nuclei are special many-body systems which are very suitable for the test of isospin symmetry [1, 2]. The reason is that they are most symmetric with respect to the proton-neutron degree of freedom and that yrast states with different isospin quantum numbers co-exist at low energy [3, 4, 5, 6, 7]. This allows  $\gamma$ -ray spectroscopy of isovector ( $T = 1$ )  $\rightarrow$  ( $T = 0$ ) transitions and it makes odd-odd  $N = Z$  nuclei important for testing isospin symmetry [2, 8]. Furthermore, these nuclei play a decisive role in the determination of the  $T = 0$  part of effective interactions, *e.g.*, [9, 10], and they are of great interest for the understanding of weak processes, enhancement mechanisms of electromagnetic transitions, as well as for problems of nuclear astrophysics [11, 12].

However, up to very recent time more or less comprehensive information was available only for the odd-odd  $N = Z$  nuclei in the  $p$ -,  $sd$ - shells and for one nucleus from the  $pf$ -shell:  $^{42}\text{Sc}$ . Recent progress in both experimental and theoretical directions brought new valuable data for the heavy odd-odd  $N = Z$  nuclei  $^{46}\text{V}$  [4, 5, 6, 13, 14, 15, 16],  $^{50}\text{Mn}$  [7, 17, 18, 19, 20, 21], and  $^{54}\text{Co}$  [22, 23, 24, 25] in the lower part of the  $pf$ -shell ( $f_{7/2}$ -shell) and even for some nuclei of the upper part of the  $pf$ -shell, like  $^{70}\text{Br}$  [26, 27]. While some understanding of the key problems of the low-energy structure of  $f_{7/2}$  nuclei seems to be obtained and regulari-

ties similar to the ones appropriate for the  $sd$ -shell are revealed there are still many uncertainties for low-spin structure of these nuclei with mass numbers  $A > 56$  [28, 29, 30, 31, 32, 33, 34, 35]. The first odd-odd  $N = Z$  nucleus of this region, which may help to draw confident conclusions on the situation in the mass region above  $^{56}\text{Ni}$  is  $^{58}\text{Cu}$ . But the experimental data available for the low-energy level scheme of  $^{58}\text{Cu}$  [36, 37, 38, 39, 40, 41] is quite sparse and the theoretical full- $pf$  shell model treatment of this nucleus is a tough computational problem. Early attempts to understand the low-spin level scheme of  $^{58}\text{Cu}$  were, therefore, limited to shell model calculations with the inert  $^{56}\text{Ni}$  core. This approach unsatisfactorily required substantial changes in the values of single particle energies with respect to the ones for the  $f_{7/2}$  nuclei and too large effective quadrupole charges [42, 43].

This paper presents new experimental data for  $^{58}\text{Cu}$  which was investigated with the  $^{58}\text{Ni}(p,n\gamma)^{58}\text{Cu}$  fusion evaporation reaction up to an excitation energy of 3.5 MeV with the Cologne OSIRIS cube  $\gamma$ -array. We could significantly extend the hitherto known low spin level scheme of  $^{58}\text{Cu}$  [36, 37, 38, 39], identify many new transitions, and establish their multipole character and relative intensities. The new experimental results are accompanied by full  $pf$ -shell model calculations with the new GXPF1 residual interaction [44] universal for the whole  $pf$ -shell and help to verify experimental assignments. The data and the GXPF1 results are compared to schematic shell model calculations with the  $^{56}\text{Ni}$  core

and a residual surface delta interaction (SDI). The consequences of the softness of the  $^{56}\text{Ni}$  core on the spectra are pointed out.

## II. EXPERIMENTAL DETAILS AND RESULTS

Excited states of  $^{58}\text{Cu}$  were populated in the  $^{58}\text{Ni}(p,n\gamma)^{58}\text{Cu}$  fusion evaporation reaction with a beam energy of 14 MeV provided by the Cologne FN-TANDEM accelerator. The target was a 1 mg/cm<sup>2</sup> thick highly enriched self-supporting  $^{58}\text{Ni}$  foil. Five Compton-suppressed Ge-detectors and one Compton-suppressed EUROBALL CLUSTER detectors [45] were used in the Cologne OSIRIS cube-spectrometer. Two of the Ge-detectors were mounted in forward direction at an angle  $\theta = 45^\circ$  with respect to the beam axis. Another two were mounted in the backward direction at an angle of  $\theta = 135^\circ$  with respect to the beam axis. The fifth Ge-detector and the EUROBALL CLUSTER detector were placed at an angle  $\theta = 90^\circ$  below and above the beam line, respectively. About  $10^9$   $\gamma\gamma$ -coincidence events were recorded. Single  $\gamma$  spectra and  $\gamma\gamma$  coincidence spectra of the depopulating photon cascades in  $^{58}\text{Cu}$  were measured with high energy resolution. As an example of the data, Fig. 1 shows the  $\gamma$  spectrum observed in coincidence with the decay of the  $J^\pi = 3^+$ ,  $T = 0$  state to the  $J^\pi = 1^+$ ,  $T = 0$  ground state of  $^{58}\text{Cu}$ . The low-spin level scheme of  $^{58}\text{Cu}$  was constructed from the  $\gamma\gamma$  coincidence relations. It is displayed in Fig. 2. We observed 17 levels and 31  $\gamma$  transitions in this nucleus. With respect to earlier spectroscopic work [36, 37, 38, 39], 17  $\gamma$  transitions and five levels are new. In order to assign spin and parity quantum numbers we analyzed the  $\gamma\gamma$  angular correlation information and the signs of linear polarizations using the EUROBALL CLUSTER detector as a Compton polarimeter. The angular correlation pattern is determined by the spin quantum numbers of the levels involved in a cascade, by the Gaussian width  $\sigma$  of the  $m$ -substate distribution of the initial level and by the multipole character of the corresponding  $\gamma$  radiation. The Gaussian width  $\sigma$  [46] and multipole mixing ratio  $\delta$  have been deduced from  $\chi^2$  minimization [47]. The sign convention following Krane, Steffen and Wheeler [48] has been used for the determination of  $\delta$ .

The analysis of the  $\gamma\gamma$  angular correlations resulted in five new unambiguous spin assignments for the levels at 444 keV ( $J^\pi = 3^+$ ), 1052 keV ( $J^\pi = 1^+$ ), 2066 keV ( $J^\pi = 5$ ), 2751 keV ( $J = 4$ ) and 3423 keV ( $J^\pi = 7$ ). The spin assignments for the levels at 2066 keV ( $J^\pi = 5$ ) and 3423 keV ( $J^\pi = 7$ ) are based on the spin and parity assignment  $J^\pi = 3^+$  of the level at 444 keV. The assignment for the level at 1653 keV ( $J^\pi = 2^+$ ) has been confirmed in the present experiment.

As an example for the assignments we show in Fig. 3 the experimental values of the relative  $\gamma\gamma$  coincidence intensities of the 1103 – 1648 keV cascade for the angular correlation groups of our spectrometer together with the

values fitted for two different spin hypotheses. The number of different correlation groups results from the geometry of the COLOGNE-COINCIDENCE-CUBE-spectrometer [49]. The 1103 – 1648 keV cascade connects the level at 1648 keV, which could be assigned  $J^\pi = 3^+$  via the angular correlation of the 1204 – 444 keV cascade, with the  $J^\pi = 1^+$  ground state. It is evident from the figure, that a spin quantum number  $J = 5$  for the level at 2751 keV can not reproduce the data ( $\chi_{min}^2 = 15.8$ ) for any value of the possible octupole/quadrupole mixing ratio  $\delta$  of the assumed  $5 \rightarrow 3^+$  transition. In contrast to this the fitted values are in good accordance with the experimental ones ( $\chi_{min}^2 = 1.1$ ) for a spin quantum number  $J = 4$  for the level at 2751 keV. For the correlation analysis we treat the parameter,  $\sigma$ , which describes the Gaussian width of the  $m$ -substate distribution, as a free parameter. Aside from the spin quantum numbers of the excited states, the measured  $\gamma\gamma$  angular correlations also give valuable information on the multipole mixing ratios of the  $\gamma$  transitions involved (see Table I).

For seven levels with known spin values, we could also deduce the parity. This assignment was based on the electric or magnetic character of the depopulating  $\gamma$ -transitions. To determine this character, the CLUSTER detector was used as a Compton polarimeter. The sum of two coincident detector signals, which stem from the Compton scattering of an initial  $\gamma$ -quantum in one segment of the CLUSTER and the subsequent absorption in another segment, carries the full energy information of the initial  $\gamma$ -ray. The geometry of the Compton scattering process depends on the polarization of the initial  $\gamma$ -ray with respect to the beam axis. Therefore observable asymmetries of the Compton scattering process allow to measure the  $\gamma$ -polarizations and the radiation character.

The seven large volume Ge-crystals of the CLUSTER form a non-orthogonal polarimeter. Numerical simulations [50] as well as recent experiments [7, 23, 51] have shown, that the CLUSTER detector is an efficient Compton polarimeter. The in-set in Fig. 4 shows the configuration of the CLUSTER with respect to the beam axis in the present experiment. This configuration leads to three different scattering planes for the Compton scattering of  $\gamma$ -rays between adjacent segments of the CLUSTER. In our experiment these scattering planes enclosed angles of  $30^\circ$ ,  $90^\circ$ , and  $150^\circ$  with the reaction plane, respectively. The sum energy of the two coincident signals was sorted in two different spectra,  $N_{90^\circ}$  and  $N_{30^\circ,150^\circ}$  depending on to which scattering plane the involved pair of segments corresponds. These spectra were used to obtain proper spectra for Compton scattering intensity differences and sums, namely,  $N_- = N_{90^\circ} - 1/2 N_{30^\circ,150^\circ}$  and  $N_+ = N_{90^\circ} + 1/2 N_{30^\circ,150^\circ}$ . The experimental asymmetry is defined as [51]

$$A_{\text{exp}} = \frac{N_-}{N_+} \approx Q^{\text{Pol}} P, \quad (1)$$

where  $Q^{\text{Pol}}$  denotes the positively defined polarization sensitivity of the CLUSTER and  $P$  is the linear polariza-

tion of the incoming photon with respect to the given geometry. Since the sign of the linear polarization,  $\text{sgn}(P)$ , determines the character of the electromagnetic radiation in case of pure multipolarity, we can conclude this character with Eq. (1) from the sign of the experimental asymmetry  $\text{sgn}(A_{\text{exp}})$ . Fig. 4 shows the difference spectrum  $N_-$ .  $N_+$  has positive values for all energies.

A summary of the energy levels with certain spin and parity values and with their depopulating  $\gamma$  transitions and branching ratios is given in Table I. The assignment of the isospin quantum number  $T = 1$  is done by comparing the energies of the levels to the energies of the corresponding states of the  $T = 1$  isobaric partner nucleus  $^{58}\text{Ni}$ .

From isospin symmetry we expect, that the excitation energies of analogue states are close in isobaric partners. The two lowest excited states in  $^{58}\text{Ni}$  are the  $J^\pi = 2_1^+$  state at 1454 keV and the  $J^\pi = 4_1^+$  state at 2460 keV. From the excitation energy of the  $2_1^+$  state in  $^{58}\text{Ni}$  and from the difference of excitation energies (1450 keV) of the  $0_1^+, T = 1$  state (203 keV) and the  $2_2^+$  state (1653 keV) in  $^{58}\text{Cu}$  one can assign the isospin quantum number  $T = 1$  to the  $2_2^+$  state in  $^{58}\text{Cu}$ . Furthermore the large  $M1$  matrix elements of the 601.4 keV and 1208.8 keV transitions to the  $1_2^+$  and  $3_1^+$ ,  $T = 0$  states, respectively, and the predominantly isovector character of the  $M1$  transition operator support the  $T = 1$  assignment.

Assuming positive parity for the  $J = 4$  state of  $^{58}\text{Cu}$  at 2751 keV excitation energy, it can be tentatively identified as the IAS of the  $J^\pi = 4_1^+, T = 1$  state of  $^{58}\text{Ni}$ . Similar to the case of the  $2_2^+$  state, this assignment is again based on the comparison of the excitation energy difference (2548 keV) to the  $0_1^+, T = 1$  state at 203 keV with the excitation energy of the  $J^\pi = 4_1^+$  state of  $^{58}\text{Ni}$  and on the  $\gamma$ -decay pattern. The decays of that  $J^\pi = 4$  state to the  $3_2^+$  and  $4_1^{(+)}, T = 0$  states is characterized by very small quadrupole/dipole mixing ratios. This fact supports the  $T = 1$  assignment for the level at 2751 keV. Although small quadrupole/dipole mixing ratios were also expected for a  $T = 1$  state with negative parity we can discard the possibility of a  $T = 1$   $4^-$  state because there are no negative parity states in  $^{58}\text{Ni}$  in this energy region. In a previous study of  $^{58}\text{Cu}$  [39] a level at 2690(20) keV was identified as the  $T = 1, J^\pi = 4^+$  state from particle spectroscopy in  $(^3\text{He}, t)$  charge exchange reactions. Its  $T = 1$  assignment was done in Ref. [39] on the basis of the close energy match to the  $4_1^+$  state of the isobaric partner nucleus  $^{58}\text{Ni}$ . This state was not observed in the present experiment and its decay properties are not known. Due to the comparably large uncertainty for the excitation energies deduced from that particle spectroscopy the values of energies from the previous and the present paper for the assigned  $4^+$  states at about 2.7 MeV agree within three standard deviations. Therefore, one might think that the uncertainty in excitation energy of 2690(20) keV claimed by the authors of Ref. [39] could have been too optimistic for that particular level

and their  $T = 1, J^\pi = 4^+$  state would coincide with the  $T = 1, J^\pi = 4^+$  state at 2751 keV proposed above. It is, however, also possible that there exists a doublet of  $4^+$  states, one with isospin quantum number  $T = 1$  and the other with  $T = 0$  as it was recently observed in the neighboring odd-odd  $N = Z$  nucleus  $^{54}\text{Co}$  [8]. The latter hypothesis is supported by the shell model results discussed in the next section.

### III. DISCUSSION

One of the first successful and very important results of the nuclear shell model was an understanding of the origin of the  $N = Z = 28$  magic number. Thus, the nucleus  $^{56}\text{Ni}$  has the properties of a doubly magic inert core in a simple approach of spherical shell model. This assumes that the low-energy structure of  $A > 56$  nuclei with several nucleons above  $^{56}\text{Ni}$  may be described within the shell model in small configurational spaces.  $^{58}\text{Cu}$  is one of such nuclei and shell model calculations with a  $^{56}\text{Ni}$  core have been performed for this nucleus already in the late 1960's [42, 43]. However, it was realized that the excitations of  $^{56}\text{Ni}$  core are important for the structure of the nuclei with  $A > 56$  [52, 53]. The recent information on  $^{56}\text{Ni}$  [54, 55] establishes a rather high degree of softness of  $^{56}\text{Ni}$ . Core excitations are important and can be described by modern large-valence shell calculations. In fact, it has been found that a recent effective interaction suitable for mid- $pf$ -shell nuclei produces a significant amount of  $^{56}\text{Ni}$  core excitations in neighbor nuclei of about 30 - 40% [44, 56]. One way to identify the impact of the core excitations on the structure of  $^{58}\text{Cu}$  is to compare the predictions of modern large-scale shell model calculations with an effective interaction adjusted for the full  $pf$ -shell – which include the core excitations – with small space shell model calculations with an inert  $^{56}\text{Ni}$  core and a schematic interaction suitable for the smaller  $pf_{5/2}$  space – that do not contain the core excitations.

We have, therefore, performed two sets of shell model calculations for  $^{58}\text{Cu}$ . The first one uses  $^{56}\text{Ni}$  as the core and a residual surface delta interaction (SDI) [57] with a parameterization similar to the one for  $^{54}\text{Co}$  [8]. Single particle energies were extracted further from the spectrum of  $^{57}\text{Ni}$  (see Table II). The resulted excitation energies are compared to the experimental spectra in Fig. 5. We note that there is a good agreement for the two lowest states of each spin value  $J$ , except for the  $3_1^+$  and the  $5_1^+$  state for which the calculated energies are 0.5 MeV higher than the experimental ones. We have calculated also  $B(M1)$  and  $B(E2)$  values between the low-lying states which are shown in Table III.

The second set of calculations was performed by the Tokyo group with the new effective GXPF1 interaction [44]. This interaction (195 two-body matrix elements and 4 single particle energies) was determined partly from a fit to 699 experimental binding energies and level energies

from 87 nuclei with  $A \geq 47$  and  $Z \leq 32$ . The starting point for the fitting procedure was a realistic G-matrix interaction with core-polarization corrections based on the Bonn-C potential. Thus, for the first time a universal effective interaction for the whole  $pf$ -shell is determined.

The calculation with the GXPF1 interaction was performed in the full  $pf$  shell with up to 6-particle excitations from the  $f_{7/2}$  orbital to the  $p_{3/2}$ ,  $p_{1/2}$  and  $f_{5/2}$  orbitals. Results for the excitation energies are compared to the experimental data in Fig. 6. One may note quite good reproduction of the experimental data. In contrast to the calculations with the inert  $^{56}\text{Ni}$  core (see Fig. 5) there are also states with  $J > 5$  which are entirely due to the breaking of the  $^{56}\text{Ni}$  core. They are coming mainly from a coupling of the one-neutron-one-proton states to the first excited  $2^+, T = 0$  state at 2.7 MeV in the  $^{56}\text{Ni}$  core. The energies of the  $J^\pi = 7_{1,2}^+$  and  $J^\pi = 8_1^+$  states are perfectly reproduced indicating that the core excitations are correctly taken into account. Furthermore there is a much better agreement for the  $J^\pi = 3_1^+$  and the  $J^\pi = 5_1^+$  states. It has to be emphasized also a very good reproduction of the excitation energies and an ordering of the  $4_2^+, T = 0$  and the  $4_3^+, T = 1$  states which form isospin doublet. The electromagnetic transition strengths and lifetimes calculated with GXPF1 are compared also to the available experimental data in Table III.

It is interesting to compare the two sets of calculations. The excitation energies of the yrast low-lying states with  $J \leq 5$  are reproduced excellently by the GXPF1 and acceptable for the SDI interaction. The mean level deviations are 41 keV and 83 keV, respectively. Furthermore the single particle energies (s.p.e.) used for the SDI with the  $^{56}\text{Ni}$  core and the effective s.p.e. from GXPF1 for the  $^{56}\text{Ni}$  core are rather similar. However, switching to electromagnetic transition strengths we find many differences (see columns Th-1 and Th-2a, Th-2b of Table III).

First, we note that to reproduce the experimental  $B(E2; 2^+, T = 1 \rightarrow 0^+, T = 1)$  value in the calculations with the  $^{56}\text{Ni}$  core we have to increase the sum of the effective quadrupole charges  $e_p + e_n$  by a factor of 2 as compared to the GXPF1 charges. This causes also other  $\Delta T = 0$   $E2$  transitions to become enhanced some of them even exceeding the corresponding large  $B(E2)$  values from the GXPF1 calculations, *e.g.* like the  $E2$  decays of the  $1_2^+$  state.

Second, favored isovector  $\Delta T = 1$   $M1$  transitions are of special interest, while isoscalar  $M1$ 's are strongly suppressed and usually carry less information on the structure of the wave functions. In the simple quasideuteron picture [58] one expects a strong enhancement of  $0^+, T = 1 \rightarrow 1^+, T = 0$  transitions (up to  $7.3 \mu_N^2$  with spin-quenching of 0.7) for  $^{58}\text{Cu}$  because of the firm presence of the  $p_{3/2}$  orbital. Indeed, in the calculations with the  $^{56}\text{Ni}$ -core, which closer matches the quasi-deuteron scheme, the summed  $B(M1)$  strength for the lowest two  $1^+$  states amounts to  $5.7 \mu_N^2$ . The inclusion of core excitations reduces this sum to  $2.5 \mu_N^2$ . The distribution

of this  $M1$  strength among these two lowest  $1^+$  states is different for the two sets of calculations, too. The  $B(M1; 0_1^+ \rightarrow 1_1^+)$  values are rather similar in both calculations, but the  $B(M1; 1_2^+ \rightarrow 0_1^+)$  values differ by a factor of 5 even for the quenching of 0.7 for the SDI. Since the calculations with the Ni core are in a very small configurational space one expects larger  $B(M1)$  values as compared to the large scale shell model. This is correct for the  $B(M1; 1_2^+ \rightarrow 0_1^+)$  value but not for the  $B(M1; 0_1^+ \rightarrow 1_1^+)$  value. Furthermore, the comparison of the  $E2$  strengths for the  $2_1^+ \rightarrow 1_1^+$  and  $2_1^+ \rightarrow 1_2^+$  transitions yields an apparent inversion of the  $1_1^+$  and  $1_2^+$  states in the SDI calculation with respect to the GXPF1 results. The latter yields almost the same  $B(E2)$  ratio for these two transitions as the experimental one. The  $B(E2; 3_2^+ \rightarrow 1_{1,2}^+)$  values allow to draw the same conclusion. This inversion of the  $1^+$  states and the considerable reduction of the  $M1$  strengths are caused by the core excitations.

Most interesting are, however, the isovector  $M1$  strengths for the  $2_2^+ \rightarrow 1_1^+$  and  $2_2^+ \rightarrow 1_2^+$  transitions. Their ratio also indicates the inversion of the  $T = 0$   $1^+$  states: for the GXPF1 calculations the stronger transition goes to the  $1_2^+$  state, while for the SDI interaction it is the transition to the  $1_1^+$  state. The latter should be almost completely forbidden according to the GXPF1 result. The  $M1$  strengths for the isovector  $2_2^+ \rightarrow 3_1^+$ ,  $2_2^+ \rightarrow 2_1^+$ ,  $4_3^+ \rightarrow 3_2^+$ , and  $4_2^+ \rightarrow 4_1^+$  transitions indicate that many  $B(M1)$  values even from the GXPF1 calculations are significantly stronger than the isovector  $4_3^+ \rightarrow 3_1^+$  or  $2_2^+ \rightarrow 1_1^+$  transitions by two to four orders of magnitude. A suppression of an isovector  $M1$  transition by four orders of magnitude could indicate the presence of a powerful selection rule being at work.

We propose that this hindrance of the  $2_2^+ \rightarrow 1_1^+$  transition is a consequence of a  $Q$ -phonon [59, 60, 61] selection rule applied here to  $M1$  transitions in the shell model. The reasoning if this interpretation is sketched in Fig. 7. In the shell model calculation with the GXPF1 interaction the  $T = 1$   $2_2^+$  state is most dominantly a complex one-quadrupole phonon excitation of the  $T = 1$   $0_1^+$  state, *i.e.*, to a good approximation  $|2^+, T = 1\rangle \propto Q|0^+, T = 1\rangle$  where  $Q$  denotes the isoscalar quadrupole operator. The  $T = 0$   $1_1^+$  state's wave function is instead generated to a large extent from the action of a part  $\Delta$  of the isovector  $M1$  transition operator on the  $T = 1$   $0_1^+$  state,  $|1^+, T = 0\rangle \propto \Delta|0^+, T = 1\rangle$ . Consequently, the  $2_2^+ \rightarrow 1_1^+$  transition represents a two-step process. The one-body  $M1$  transition operator cannot simultaneously annihilate the  $2_2^+ \rightarrow 0_1^+$   $Q$ -phonon and cause the  $0_1^+ \rightarrow 1_1^+$   $M1$  transition. Therefore, the  $2_2^+ \rightarrow 1_1^+$   $M1$  transition is strongly hindered which is well confirmed by the data. This interpretation is supported by the strong  $2_2^+ \rightarrow 3_1^+$ ,  $\Delta T = 1$   $M1$  transition, which is allowed in the  $Q$ -phonon scheme if we consider the  $3_1^+$  state as a  $Q$ -phonon excitation of the  $1_1^+$  state. For this  $2_2^+ \rightarrow 3_1^+$  transition one  $Q$ -phonon excitation is present in both, the initial and the final state, and acts as a spectator. Indeed, the  $B(M1)$  values

for the  $2_2^+ \rightarrow 3_1^+$  and  $0_1^+ \rightarrow 1_1^+$  transitions calculated with the GXPF1 interaction are close. It is of interest to analyze these observations from the viewpoint of symmetries discussed in [62, 63].

#### IV. CONCLUSION

In summary we have investigated the low spin states of the odd-odd  $N = Z$  nucleus  $^{58}\text{Cu}$  with the  $^{58}\text{Ni}(p,n\gamma)^{58}\text{Cu}$  fusion evaporation reaction. In the present experiment 17 low spin states were observed. Five of them and 17 new  $\gamma$ -ray transitions were observed for the first time. Numerous multipole mixing ratios and branching ratios were determined and 5 new spin assignments were made. The new data helps to understand the role of core excitations for the low-spin structure of  $^{58}\text{Cu}$ .

We have performed shell model calculations for the low-lying states of  $^{58}\text{Cu}$  with the SDI residual interaction with a  $^{56}\text{Ni}$  core and with the new GXPF1 interaction which is universal for the whole pf-shell. Comparison of the experimental excitation energies to the corresponding experimental quantities shows that both calculations yield good agreement for the yrast states with  $J \leq 5$ . However the results of the two calculations differ considerably for electromagnetic transition strengths and the agreement with experiment is much better for the full- $pf$  shell calculations. In particular, we note that the  $B(E2)$  values for isoscalar transitions are enhanced by a factor of 4 and the isovector  $B(M1)$  values are reduced by factor 5-10 for the full calculation as compared to the  $pf_{5/2}$  space. Big changes in the electromagnetic transition strengths indicate the important role of  $^{56}\text{Ni}$  excitations for the structure of the low-spin states of  $^{58}\text{Cu}$ . The apparent hindrance of the  $(T = 1) \rightarrow (T = 0)$  isovector  $2_2^+ \rightarrow 1_1^+$

$M1$  transition is well reproduced by the GXPF1 interaction and can be interpreted as the manifestation of a  $Q$ -phonon selection rule for  $M1$  transitions in the shell model.

Another interesting result is the suggested existence of a  $T = 0$  and  $T = 1$  doublet of  $4^+$  states at  $\approx 2.7$  MeV. The comparison of data with the calculations favor the  $4^+$  state at 2.751 MeV to have isospin  $T = 1$ . It would be interesting to find  $\gamma$ -transitions from the nearby  $4^+, T = 0$  state predicted by the shell model and ambiguously suggested in [39] at  $\approx 2.69(2)$  MeV as the lowest  $4^+, T = 1$  state of  $^{58}\text{Cu}$ . The identification and study of this isospin doublet may offer valuable information on the isospin breaking for nuclei along the  $N = Z$  line above  $^{56}\text{Ni}$ .

#### V. ACKNOWLEDGMENT

The authors want to thank in particular A. Fitzler, S. Kasemann, and H. Tiesler for help in data taking. We also thank A. Dewald, J. Eberth, A. Gelberg, J. Jolie, R.V. Jolos, D. Rudolph, D. Weißhaar, and K.O. Zell for helpful discussions. This work was supported in part by the DFG under support No. Pi 393/1-2, No. Br - 799 /10-2, the U.S. National Science Foundation Grant No. PHY-0070911 and Grant-in-Aid for Specially Promoted Research (13002001) from the Ministry of Education, Science, Sport, Culture and Technology of Japan. We mention that this work is originated in a JSPS-DFG joint project. The large-scale numerical calculations were performed on parallel computers at the Center for Nuclear Study (CNS) at the University of Tokyo supported by the Grant above mentioned and also by the CNS-RIKEN joint project for large-scale nuclear structure calculations.

- 
- [1] D. H. Wilkinson, *Isospin in Nuclear Physics* (North Holland Publishing Company, Amsterdam, 1969).
- [2] A. P. Zuker, S. M. Lenzi, G. Martinez-Pinedo, A. Poves, Phys. Rev. Lett. **89** 142502 (2002).
- [3] P. Vogel, Nucl.Phys. A662, 148 (2000).
- [4] C. Frießner, N. Pietralla, A. Schmidt, I. Schneider, Y. Utsuno, T. Otsuka, and P. von Brentano, Phys. Rev. C **60**, 011304 (1999).
- [5] S. M. Lenzi, D. R. Napoli, C. A. Ur, D. Bazzacco, F. Brandolini, J. A. Cameron, E. Caurier, G. de Angelis, M. De Poli, E. Farnea, A. Gadea, S. Hankonen, S. Lunardi, G. Martinez-Pinedo, Zs. Podolyak, A. Poves, C. Rossi Alvarez, J. Sanchez-Solano, H. Somacal, Phys. Rev. C **60**, 021303 (1999).
- [6] C. D. O'Leary, M. A. Bentley, D. E. Appelbe, R. A. Bark, D. M. Cullen, S. Erturk, A. Maj, J. A. Sheikh, D. D. Warner, Phys. Lett. **459B**, 73 (1999).
- [7] A. Schmidt, I. Schneider, C. Frießner, A.F. Lisetskiy, N. Pietralla, T. Sebe, T. Otsuka, and P. von Brentano, Phys. Rev. C **62**, 044319 (2000).
- [8] A. F. Lisetskiy, A. Schmidt, I. Schneider, C. Friessner, N. Pietralla and P. von Brentano, Phys. Rev. Lett. **89**, 012502 (2002).
- [9] I. Talmi, Rev. Mod. Phys. 34, 704 (1962) .
- [10] J. D. McCullen, B. F. Bayman, L. Zamick, Phys. Rev. 134, B515 (1964).
- [11] I. S. Towner, J. C. Hardy, Phys.Rev. C**66**, 035501 (2002).
- [12] B. A. Brown, Prog. Part. Nucl. Phys. 47, 517 (2001) .
- [13] F. Brandolini, N. H. Medina, R. V. Ribas, S. M. Lenzi, A. Gadea, C. A. Ur, D. Bazzacco, R. Menegazzo, P. Pavan, C. RossiAlvarez, A. Algora-Pineda, G. de Angelis, M. De Poli, E. Farnea, N. Marginean, T. Martinez, D. R. Napoli, M. Ionescu-Bujor, A. Iordachescu, J. A. Cameron, S. Kasemann, I. Schneider, J. M. Espino, J. Sanchez-Solano, Phys. Rev. C**64**, 044307 (2001).
- [14] P. von Brentano, A. F. Lisetskiy, A. Dewald, C. Friessner, A. Schmidt, I. Schneider, N. Pietralla, Nucl. Phys. **A682**, 48c (2001).
- [15] P. von Brentano, A. F. Lisetskiy, C. Friessner, N. Pietralla, A. Schmidt, I. Schneider, R. V. Jolos, T. Otsuka, T. Sebe, Y. Utsuno, Prog. Part. Nucl. Phys. 46, 197 (2001).

- [16] O. Möller, K. Jessen, A. Dewald, A. F. Lisetskiy, P. von Brentano, A. Fitzler, J. Jolie, A. Linnemann, B. Saha, and K. O. Zell, *Phys. Rev. C* **67**, 011301(R) (2003).
- [17] C. E. Svensson, S. M. Lenzi, D. R. Napoli, A. Poves, C.A. Ur, D. Bazzacco, F. Brandolini, J. A. Cameron, G. de Angelis, A. Gadea, D. S. Haslip, S. Lunardi, E. E. Maqueda, G. Martínez-Pinedo, M. A. Nagarajan, C. Rossi-Alvarez, A. Vitturi, and J. C. Waddington, *Phys. Rev. C* **58**, R2621 (1998).
- [18] A. F. Lisetskiy, A. Gelberg, R. V. Jolos, N. Pietralla, P. von Brentano, *Phys. Lett.* **512B**, 290 (2001).
- [19] C. D. O’Leary, M. A. Bentley, S. M. Lenzi, G. Martínez-Pinedo, D. D. Warner, A. M. Bruce, J. A. Cameron, M. P. Carpenter, C. N. Davids, P. Fallon, L. Frankland, W. Gelletly, R. V. F. Janssens, D. T. Joss, C. J. Lister, P. H. Regan, P. Reiter, B. Rubio, D. Seweryniak, C. E. Svensson, S. M. Vincent, S. J. Williams, *Phys. Lett.* **525B**, 49 (2002).
- [20] N. Pietralla, R. Krücken, C. J. Barton, C. W. Beausang, M. A. Caprio, R. F. Casten, J. R. Cooper, A. A. Hecht, J. R. Novak, N. V. Zamfir, A. Lisetskiy, A. Schmidt, *Phys. Rev. C* **65**, 024317 (2002).
- [21] M. Horoi, B. A. Brown, V. Zelevinsky, *Phys. Rev. C* **65**, 027303 (2002).
- [22] D. Rudolph, C. Baktash, M. J. Brinkman, M. Devlin, H.-Q. Jin, D. R. LaFosse, L. L. Riedinger, D. G. Sarantites, C.-H. Yu, *Eur. Phys. J. A* **4**, 115 (1999).
- [23] I. Schneider, A. F. Lisetskiy, C. Frießner, R. V. Jolos, N. Pietralla, A. Schmidt, D. Weißhaar, and P. von Brentano, *Phys. Rev. C* **61**, 044312 (2000).
- [24] N. Zeldes, *Phys. Lett.* **455B**, 7 (1999).
- [25] P. von Brentano, C. Friessner, R. V. Jolos, A. F. Lisetskiy, A. Schmidt, I. Schneider, N. Pietralla, T. Sebe, T. Otsuka, *Nucl. Phys. A* **704**, 115c (2002).
- [26] G. de Angelis, T. Martínez, A. Gadea, N. Marginean, E. Farnea, E. Maglione, S. Lenzi, W. Gelletly, C. A. Ur, D. R. Napoli, Th. Kroell, S. Lunardi, B. Rubio, M. Axiotis, D. Bazzacco, A. M. Bizzeti Sona, P. G. Bizzeti, P. Bednarczyk, A. Bracco, F. Brandolini, F. Camera, D. Curien, M. De Poli, O. Dorvaux, J. Eberth, H. Grawe, R. Menegazzo, G. Nardelli, J. Nyberg, P. Pavan, B. Quintana, C. Rossi Alvarez, P. Spolaore, T. Steinhardt, I. Stefanescu, O. Thelen, R. Venturelli, *Eur. Phys. J. A* **12**, 51 (2001).
- [27] D. G. Jenkins, N. S. Kelsall, C. J. Lister, D. P. Balamuth, M. P. Carpenter, T. A. Sienko, S. M. Fischer, R. M. Clark, P. Fallon, A. Gorgen, A. O. Macchiavelli, C. E. Svensson, R. Wadsworth, W. Reviol, D. G. Sarantites, G. C. Ball, J. Rikovsky Stone, O. Juillet, P. Van Isacker, A. V. Afanasjev, S. Frauendorf, *Phys. Rev. C* **65**, 064307 (2002).
- [28] S. Skoda, B. Fiedler, F. Becker, J. Eberth, S. Freund, T. Steinhardt, O. Stuch, O. Thelen, H. G. Thomas, L. Käubler, J. Reif, H. Schnare, R. Schwengner, T. Serdene, G. Winter, V. Fischer, A. Jungclaus, D. Kast, K. P. Lieb, C. Teich, C. Ender, T. Härtle, F. Kock, D. Schwalm, and P. Baumann, *Phys. Rev. C* **58**, R5 (1998).
- [29] D. Rudolph, C. J. Gross, J. A. Sheikh, D. D. Warner, I. G. Bearden, R. A. Cunningham, D. Foltescu, W. Gelletly, F. Hannachi, A. Harder, T. D. Johnson, A. Jungclaus, M. K. Kabadiyski, D. Kast, K. P. Lieb, H. A. Roth, T. Shizuma, J. Simpson, Ö. Skeppstedt, B. J. Varley, and M. Weiszflog, *Phys. Rev. Lett.* **76**, 376 (1996).
- [30] S. M. Vincent, P. H. Regan, D. D. Warner, R. A. Bark, D. Blumenthal, M. P. Carpenter, C. N. Davids, W. Gelletly, R. V. F. Janssens, C. D. O’Leary, C. J. Lister, J. Simpson, D. Seweryniak, T. Saitoh, J. Schwartz, S. Törmänen, O. Juillet, F. Nowacki, and P. Van Isacker, *Phys. Lett. B* **437**, 264 (1996).
- [31] T. Mizusaki, T. Otsuka, Y. Utsuno, M. Honma, T. Sebe, *Phys. Rev. C* **59**, R1846 (1999).
- [32] D. Rudolph, C. Baktash, M. J. Brinkman, E. Caurier, D. J. Dean, M. Devlin, J. Dobaczewski, P.-H. Heenen, H.-Q. Jin, D. R. LaFosse, W. Nazarewicz, F. Nowacki, A. Poves, L. L. Riedinger, D. G. Sarantites, W. Satula, C.-H. Yu, *Phys. Rev. Lett.* **82**, 3763 (1999).
- [33] A. O. Macchiavelli, P. Fallon, R. M. Clark, M. Cromaz, M. A. Deleplanque, R. M. Diamond, G. J. Lane, I. Y. Lee, F. S. Stephens, C. E. Svensson, K. Vetter, D. Ward, *Phys. Lett.* **480B**, 1 (2000).
- [34] T. Mizusaki, T. Otsuka, M. Honma, B. A. Brown, *Phys. Rev. C* **63**, 044306 (2001).
- [35] A. Petrovici, K. W. Schmid, A. Faessler, *Nucl. Phys.* **A689**, 707 (2001).
- [36] N. S. P. King, C. E. Moss, H. W. Baer, and R. A. Ristinen, *Nucl. Phys.* **A177**, 625 (1971).
- [37] F. D. Becchetti, W. Makofske, and G. W. Greenlees, *Nucl. Phys.* **A190**, 437 (1972).
- [38] D. F. H. Start, L. E. Carlson, D. A. Hutcheon, A. G. Robertson, E. K. Warbuton, and J. J. Weaver, *Nucl. Phys.* **A193**, 33 (1972).
- [39] H. Rudolph, and R. L. McGrath, *Phys. Rev. C* **8**, 247 (1973).
- [40] D. Rudolph, C. Baktash, J. Dobaczewski, W. Nazarewicz, W. Satula, M. J. Brinkman, M. Devlin, H.-Q. Jin, D. R. LaFosse, L. L. Riedinger, D. G. Sarantites, C.-H. Yu, *Phys. Rev. Lett.* **80**, 3018 (1998).
- [41] Y. Fujita, H. Fujita, T. Adachi, G. P. A. Berg, E. Caurier, H. Fujimura, K. Hara, K. Hatanaka, Z. Janas, J. Kamiya, T. Kawabata, K. Langanke, G. Martínez-Pinedo, T. Noro, E. Roeckl, Y. Shimbara, T. Shinada, S. Y. van der Werf, M. Yoshifuku, M. Yosoi, R. G. T. Zegers, *Eur. Phys. J. A* **13**, 411 (2002).
- [42] E. A. Phillips and A. D. Jackson, *Phys. Rev.* **169**, 917 (1968).
- [43] P. J. Brussard and P. W. M. Glaudemans, *Shell-model applications in nuclear spectroscopy* (North-Holland, Amsterdam, 1977).
- [44] M. Honma, T. Otsuka, B. A. Brown, T. Mizusaki, *Phys. Rev. C* **65**, 061301(R) (2002).
- [45] J. Eberth, H. G. Thomas, P. von Brentano, R. M. Lieder, H. M. Jäger, H. Kämmerling, M. Berst, D. Gutknecht, R. Henck, *Nucl. Instrum. Methods Phys. Res. A* **369**, 135 (1996).
- [46] T. Yamazaki, *Nucl. Data A* **3** (1967) 1.
- [47] A. Gade, I. Wiedenhöver, J. Gableske, A. Gelberg, H. Meise, N. Pietralla, and P. von Brentano, *Nucl. Phys.* **A665**, 268 (2000).
- [48] K. S. Krane, R. M. Steffen, and R. M. Wheeler, *Nucl. Data Tables* **11**, 351 (1973).
- [49] R. Wirowski, M. Schimmer, L. Eßer, S. Albers, K. O. Zell, and P. von Brentano, *Nucl. Phys.* **A586**, 427 (1994).
- [50] L. M. Garcia-Raffi, J. L. Tain, J. Bea, A. Gadea, L. Palafox, J. Rico, and B. Rubio, *Nucl. Instr. Meth.* **A359**, 628 (1995).
- [51] D. Weißhaar, diploma thesis, University of Cologne,

- (1996), unpublished.
- [52] C. R. Gould, E. C. Hagen, R. V. Poore, and N. R. Robertson, G. E. Mitchell and D. R. Tilley, *Phys. Rev. Lett.* **25**, 463 (1970).
  - [53] S. S. M. Wong and W. G. Davies, *Phys. Lett.* **28B**, 77 (1968).
  - [54] G.Kraus, P.Egelhof, C.Fischer, H.Geissel, A.Himmler, F.Nickel, G.Munzenberg, W.Schwab, A.Weiss, J.Friese, A.Gillitzer, H.J.Korner, M.Peter, W.Henning, J.P.Schiffer, B.A.Brown, J.V.Kratz, L.Chulkov, M.Golovkov, A.Ogloblin, *Phys.Scr.* **T56**, 114 (1995).
  - [55] T. Otsuka, M. Honma, T. Mizusaki, *Phys. Rev. Lett.* **81**, 1588 (1998).
  - [56] M. Honma, T. Otsuka, T. Mizusaki, B.A. Brown, in preparation.
  - [57] A. Plastino, R. Arvieu, and S.A. Moszkowsk, *Phys. Rev.* **145**, 837 (1966).
  - [58] A. F. Lisetskiy, R. V. Jolos, N. Pietralla, and P. von Brentano, *Phys.Rev. C* **60**, 064310 (1999).
  - [59] G. Siems, U. Neuneyer, I. Wiedenhover, S. Albers, M. Eschenauer, R. Wirowski, A. Gelberg, P. von Brentano, T. Otsuka, *Phys.Lett.* **320B**, 1 (1994).
  - [60] T. Otsuka and K.-H. Kim, *Phys. Rev. C* **50**, R1768 (1994).
  - [61] N. Pietralla, P. von Brentano, R. F. Casten, T. Otsuka, N. V. Zamfir, *Phys. Rev. Lett.* **73**, 2962 (1994).
  - [62] P. Van Isacker and D. D. Warner, *Phys. Rev. Lett.* **78**, 3266 (1997).
  - [63] P. Van Isacker, O. Juillet, F. Nowacki, *Phys. Rev. Lett.* **82**, 2060 (1999).





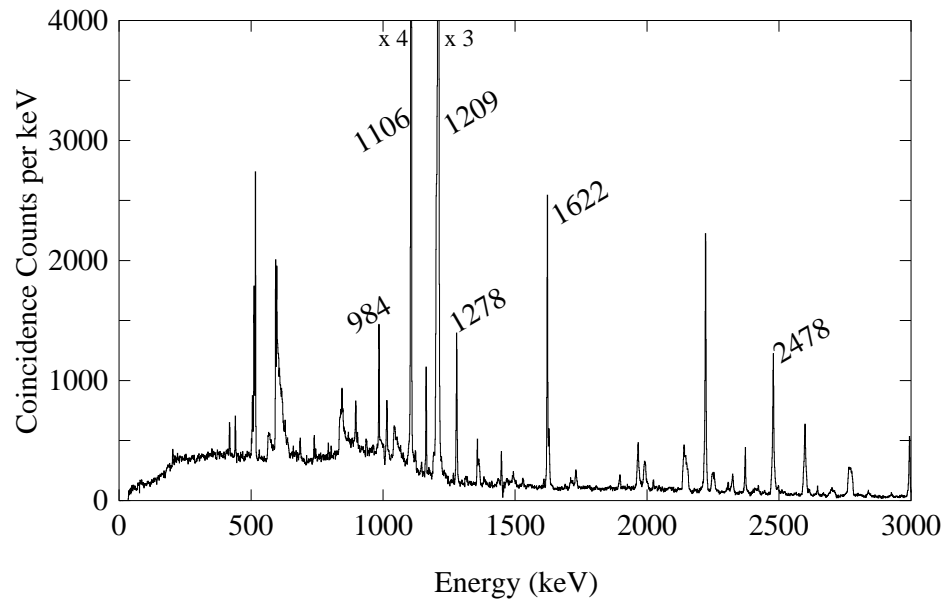


FIG. 1: The  $\gamma$ -ray spectrum is obtained by requiring a coincidence condition with the 444 keV  $3_1^+ \rightarrow 1_1^+$  transition in  $^{58}\text{Cu}$ . The numbers denote energies for transitions between states of  $^{58}\text{Cu}$  (in keV).

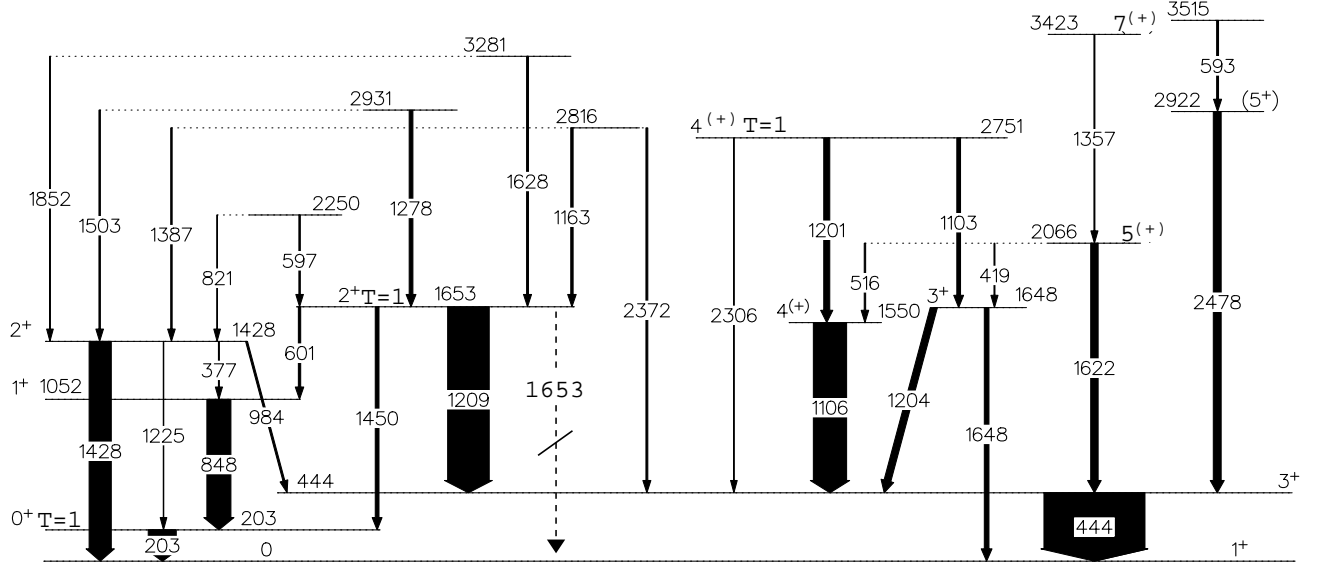
$^{58}\text{Cu}$ 

FIG. 2: Low-spin level scheme of  $^{58}\text{Cu}$  from the  $\gamma\gamma$  coincidence relations obtained in the  $^{58}\text{Ni}(p,n\gamma)^{58}\text{Cu}$  reaction at 14 MeV beam energy. Levels without an isospin label have  $T = 0$ . A possible 1653-keV  $2_2^+ \rightarrow 1_1^+$  transition marked by the dashed arrow has a branching ratio too small to have been detected (see discussion).

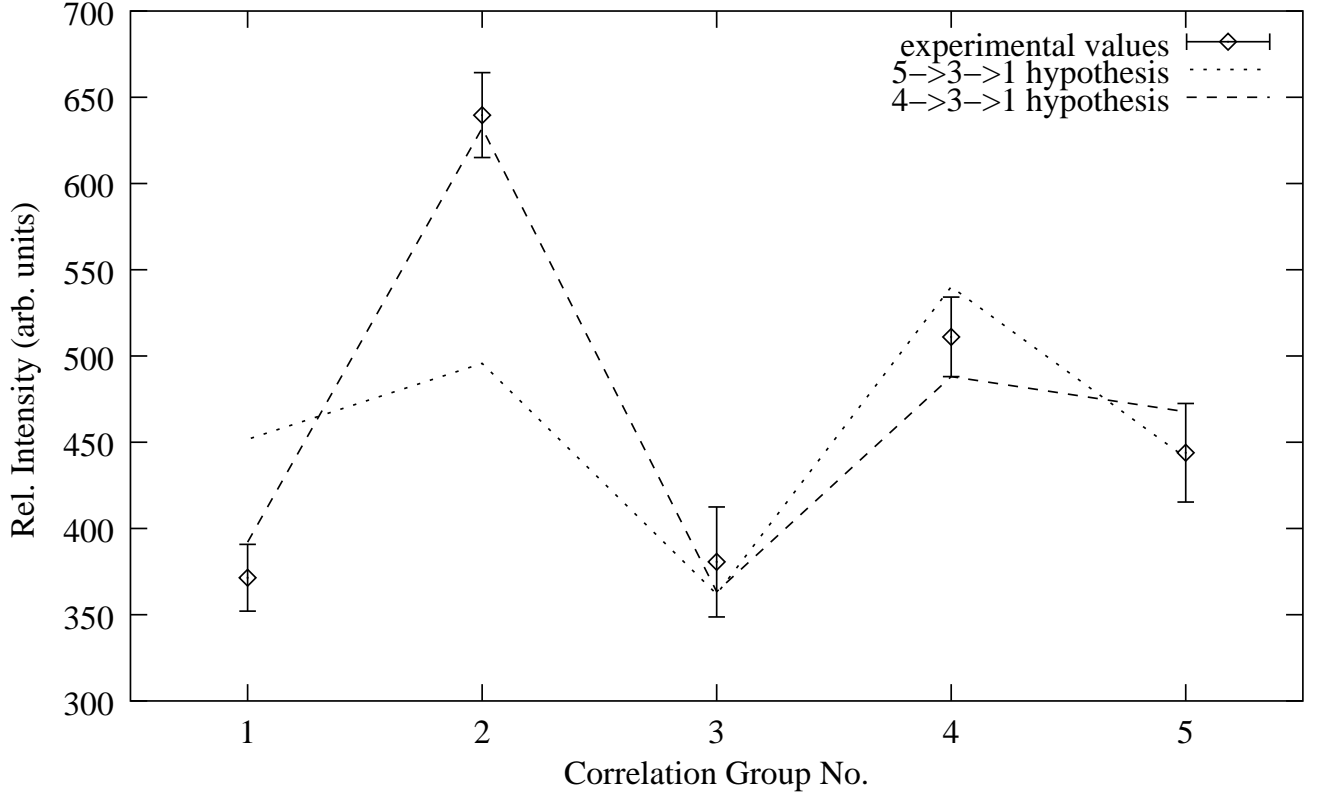


FIG. 3: Experimental and fitted values of the  $\gamma\gamma$ -angular-correlation of the 1103–1648 keV cascade which connects the  $J = 4$  level at 2751 keV with the  $J^\pi = 1^+$  ground state. Only the  $J = 4$  spin hypothesis for the upper level at 2751 keV can account for the observed correlation pattern. The fitted multipole mixing ratio for the  $4 \rightarrow 3^+$  transition is  $\delta = -0.07_{-0.12}^{+0.05}$ . The correlation group nos. label the different sets of detector pairs in the OSIRIS cube spectrometer with common sensitivities to the parameters of in-beam  $\gamma\gamma$ -angular correlation functions [49].

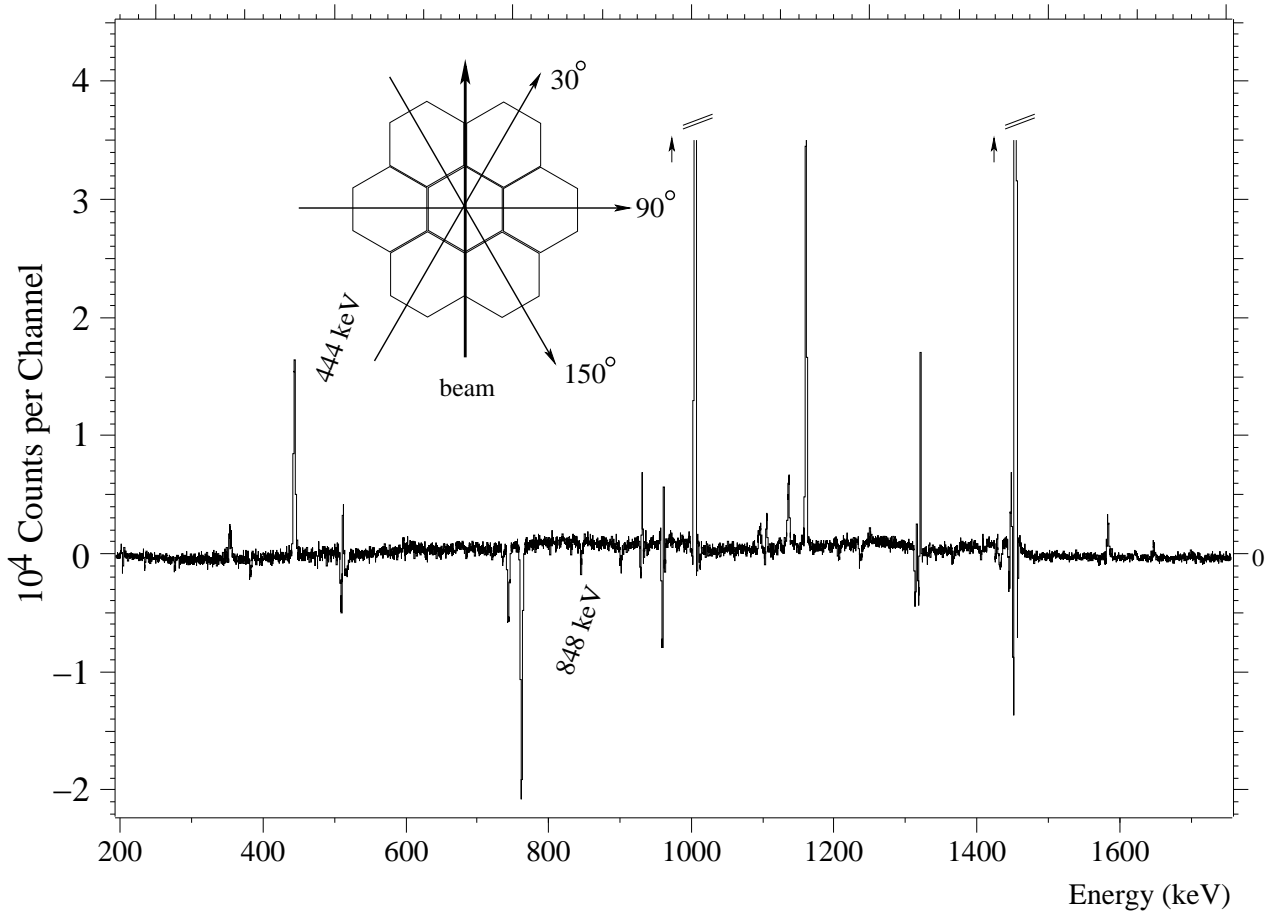


FIG. 4: Difference spectrum  $N_-$  for initial  $\gamma$ -rays, which were Compton-scattered and then fully absorbed in a pair of crystals of the composite CLUSTER detector with an orientation of  $30^\circ$ ,  $90^\circ$ , or  $150^\circ$  with respect to the beam axis, as is shown in the in-set. One expects a positive difference  $N_{90^\circ} - \frac{1}{2}(N_{30^\circ, 150^\circ})$  for electric radiation and a negative difference for magnetic radiation. The largest differences for  $\gamma$ -lines from  $^{58}\text{Cu}$  are labeled with the corresponding transition energies.

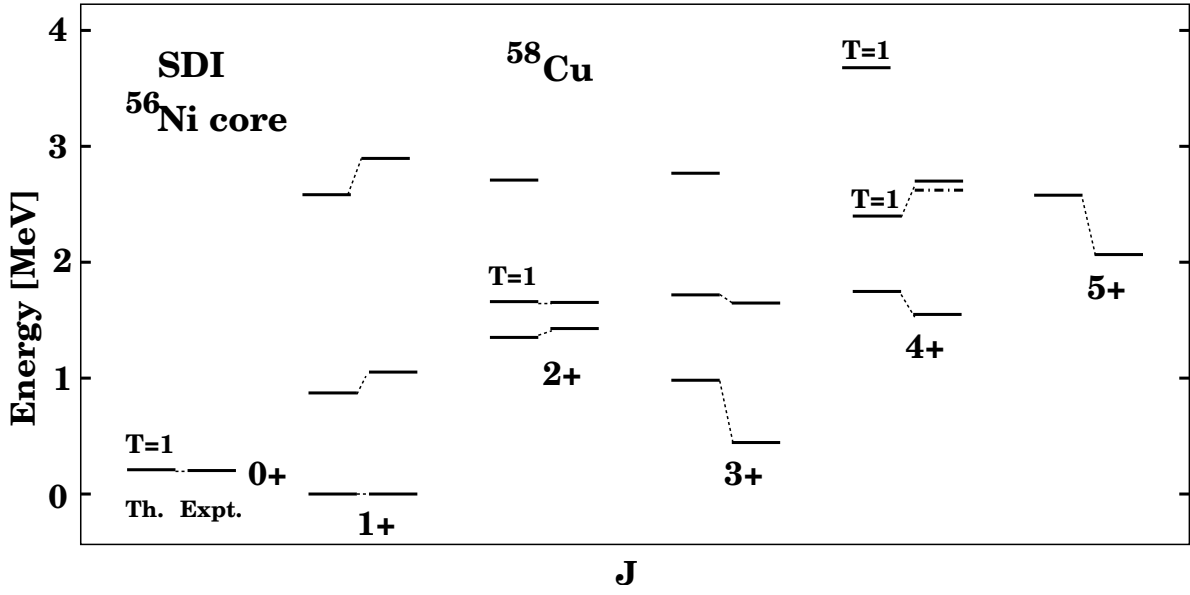


FIG. 5: Comparison of the calculated (Th.) and experimental (Expt.) excitation energies. In the shell model an inert <sup>56</sup>Ni core and two-body matrix elements of a residual SDI with parameterization and single particle energies as shown in Table II were used.

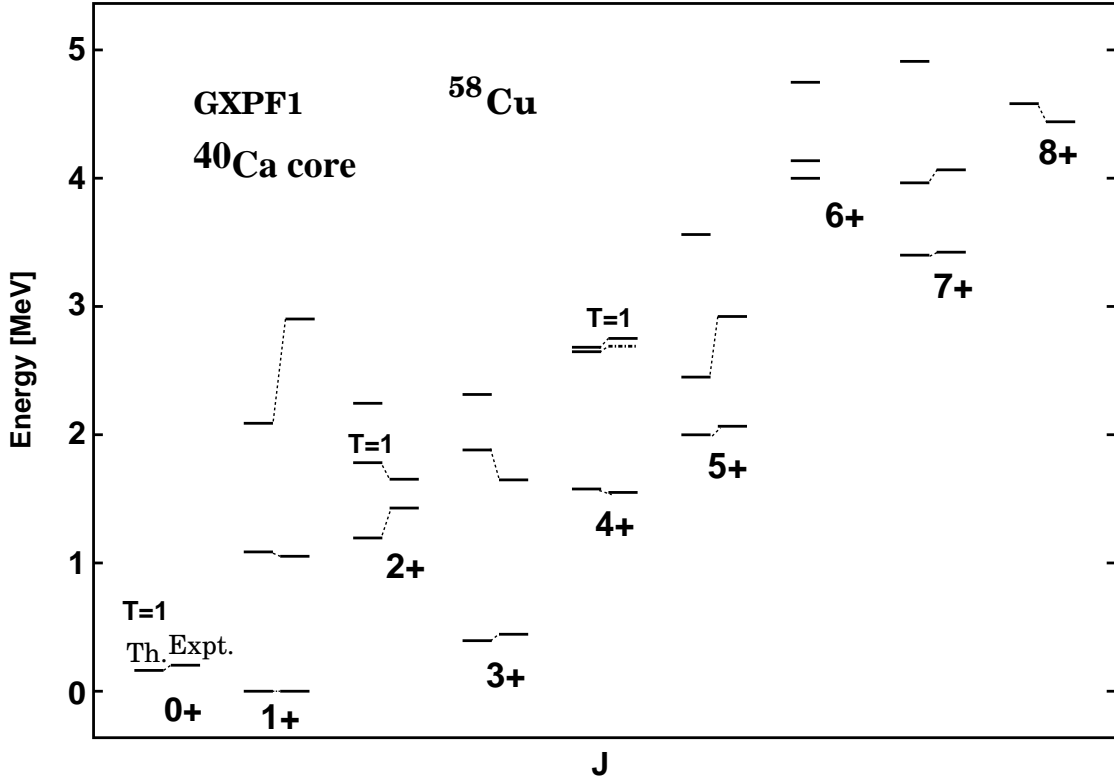


FIG. 6: Comparison of the calculated (Th.) and experimental (Expt.) excitation energies. In the shell model an inert <sup>40</sup>Ca core and two-body matrix elements of the residual GXPF1 interaction [44] and the corresponding single particle energies (see Table II) were used.

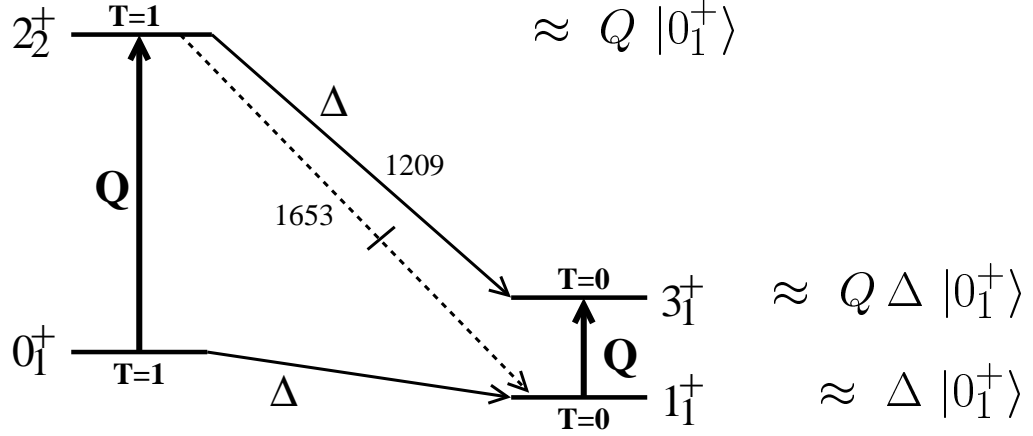
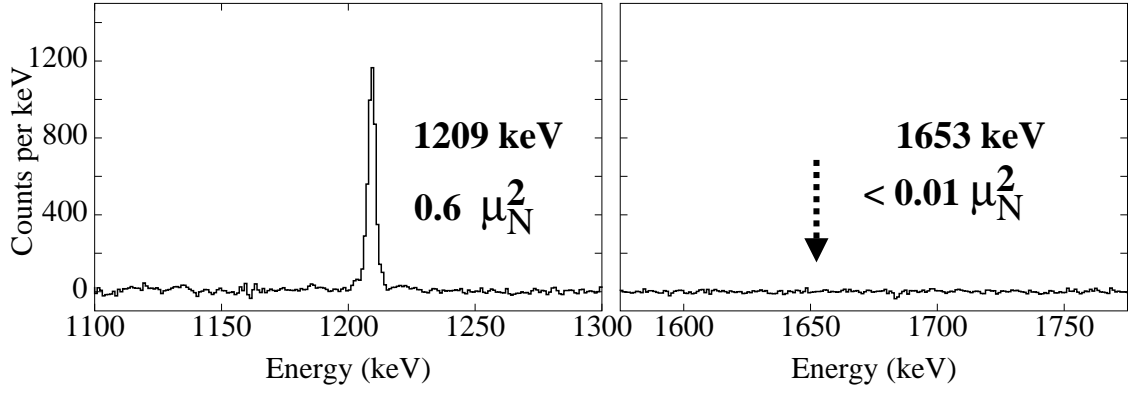


FIG. 7: Hindrance of the  $(T = 1) \rightarrow (T = 0)$  isovector  $2_2^+ \rightarrow 1_1^+$   $M1$  transition. Relevant parts of the  $\gamma$ -ray spectra in coincidence with  $\gamma$ -ray lines feeding directly the  $2_2^+$  state of  $^{58}\text{Cu}$  are displayed at the top. A strong  $2_2^+ \rightarrow 3_1^+$   $\gamma$ -ray line is visible at 1209 keV while at an energy of 1653 keV no indication for a  $2_2^+ \rightarrow 1_1^+$   $\gamma$ -ray peak was observed in the same spectrum. The intensity branching ratio is  $< 4\%$ . The  $Q$ -phonon scheme for  $M1$  transitions in the large-scale shell model interprets at the bottom the  $2_2^+ \rightarrow 1_1^+$  transition as a two-step process and, thereby, explains qualitatively its hindrance.

TABLE I: Excitation energies  $E_i$ , spin and parity quantum numbers  $I_i^\pi$  of the initial levels, the measured  $\gamma$ -transition energies  $E_\gamma$ , the excitation energy  $E_f$ , and the quantum numbers for the final levels. The last three columns denote the multipole mixing ratio  $\delta$ , the radiation character  $\mathcal{M}\ell$  ( $E$  = electric,  $M$  = magnetic), and the relative intensity ratio  $I_\gamma$ .

$E_i$ (keV)	$I_i^\pi$ $\hbar$	$\tau_i$ (fs)	$E_\gamma$ (keV)	$I_f^\pi$ $\hbar$	$\delta$	$\mathcal{M}\ell$	$I_\gamma$
0	$1_1^+$						
203	$0_1^+$		203.3	$1_1^+$		$M1$	1
444	$3_1^+$		444.3	$1_1^+$	$-0.02 \pm 0.04$	$E2$	1
1052	$1_2^+$	114(29)	608	$3_1^+$		$E2$	$< 0.043$
			848.8	$0_1^+$		$M1$	$0.935 \pm 0.065$
			1052	$1_1^+$		$E2/M1$	$< 0.087$
1428	$2_1^+$	$>966$	376.6	$1_2^+$		$E2/M1$	$0.030 \pm 0.017$
			984.2	$3_1^+$	$-0.84^{+0.21}_{-1.48}$	$E2/M1$	$0.075 \pm 0.036$
			1225.1	$0_1^+$	0	$E2$	$0.015 \pm 0.004$
			1428.3	$1_1^+$		$E2/M1$	$0.879 \pm 0.042$
1550	$4_1^{(+)}$	$>505$	1106.0	$3_1^+$	$-0.77 \pm 0.05$	$(E2/M1)$	1
1648	$3_2^+$	$>1312$	220	$2_1^+$		$E2/M1$	$< 0.034$
			1203.5	$3_1^+$	$0.53 \pm 0.13$	$E2/M1$	$0.209 \pm 0.062$
			1647.7	$1_1^+$	$-0.06^{+0.16}_{-0.27}$	$E2$	$0.791 \pm 0.062$
1653	$2_2^+$	50(10)	601.4	$1_2^+$	$0.02 \pm 0.05$	$M1$	$0.053 \pm 0.016$
			1208.8	$3_1^+$	$-0.02 \pm 0.02$	$M1$	$0.900 \pm 0.027$
			1449.5	$0_1^+$	0	$E2$	$0.048 \pm 0.016$
			1653	$1_1^+$		$E2/M1$	$< 0.037$
2066	$5_1^{(+)}$		418.6	$3_2^+$		$(M3/E2)$	$0.073 \pm 0.036$
			516.3	$4_1^{(+)}$		$(E2/M1)$	$0.167 \pm 0.063$
			1622.0	$3_1^+$	$-0.12 \pm 0.04$	$(M3/E2)$	$0.760 \pm 0.073$
2250			596.7	$2_2^+$			$0.894 \pm 0.048$
			821.3	$2_1^+$			$0.106 \pm 0.048$
2751	$4^{(+)}$		1103.1	$3_2^+$	$-0.07^{+0.05}_{-0.12}$	$(E2/M1)$	$0.397 \pm 0.081$
			1200.6	$4_1^{(+)}$	$0.00 \pm 0.05$	$(M1)$	$0.554 \pm 0.084$
			2306.4	$3_1^+$		$(E2/M1)$	$0.049 \pm 0.018$
2816			1162.7	$2_2^+$			$0.419 \pm 0.082$
			1387.2	$2_1^+$			$0.241 \pm 0.057$
			2371.5	$3_1^+$			$0.340 \pm 0.076$
2922	$(5^+)$		856	$5_1^{(+)}$		$(E2/M1)$	$< 0.028$
			1274	$3_2^+$		$(E2)$	$< 0.028$
			1372	$4_1^+$		$(E2/M1)$	$< 0.028$
			2477.5	$3_1^+$		$(E2)$	$0.959 \pm 0.041$
2931			1278.3	$2_2^+$			$0.765 \pm 0.062$
			1503.0	$2_1^+$			$0.235 \pm 0.062$
3281			1627.7	$2_2^+$			$0.843 \pm 0.053$
			1852.2	$2_1^+$			$0.157 \pm 0.053$
3423	$7^{(+)}$		1356.7	$5_1^{(+)}$		$(M3/E2)$	1
3515			592.7	$5_1^{(+)}$			1

TABLE II: The interaction parameter of the Surface Delta Interaction as defined in [43], the single particle energies (s.p.e.) of the orbits included, effective  $e_p$  and  $e_n$  charges, effective g-factors for SDI and GXPF1 as well as effective s.p.e. for GXPF1 [44]. Although, those are not parameters we show effective single-particle energies for the GXPF1 interaction in the column of the s.p.e.

Int.	s.p.e. (MeV)				Parameter values (MeV)			eff. charges		eff. g-factors			
	$\varepsilon_{f7/2}$	$\varepsilon_{p3/2}$	$\varepsilon_{\nu f5/2}$	$\varepsilon_{\nu p1/2}$	$A_{T=1}^{pp}$	$A_{T=0}^{pn}$	B	$e_p$	$e_n$	$g_i^p$	$g_i^n$	$g_s^p$	$g_s^n$
SDI (Th-2a)	-	0.00	0.83	1.88	0.50	0.45	0.16	1.50	0.50	1.00	0.00	5.59	-3.83
SDI (Th-2b)	-	0.00	0.83	1.88	0.50	0.45	0.16	2.50	1.50	1.00	0.00	3.91	-2.68
GXPF1 (Th-1)	-7.00	0.00	1.00	2.50				1.5	0.5	1.00	0.00	5.59	-3.83

TABLE III: Calculated and experimental electromagnetic transition strengths and lifetimes in  $^{58}\text{Cu}$ . The experimental energies were used for calculations of lifetimes. The results are shown for the GXPF1 interaction (Th-1) and for the SDI (Th-2a and Th-2b). Free g-factors  $g_s^{\text{eff}} = 1.0 \cdot g_s^{\text{free}}$  and effective quadrupole charges  $e_p = 1.5$ ,  $e_n = 0.5$  were used for Th-1 and Th-2a while  $g_s^{\text{eff}} = 0.7 \cdot g_s^{\text{free}}$  and  $e_p = 2.5$ ,  $e_n = 1.5$  for the Th-2b. The B(M1) values smaller than  $10^{-4}$  are replaced by 0.0. The quantities “x” and “y” are introduced for the  $5_1^+$  and the  $4_3^+$  states, respectively, in order to show experimental ratios of corresponding B(E2) or B(M1) values.

$J_i, T_i \quad J_f, T_f$	$E_i$ (MeV)			B(E2; $J_i \rightarrow J_f$ ), [ $e^2\text{fm}^4$ ]				B(M1; $J_i \rightarrow J_f$ ), [ $\mu_N^2$ ]				Lifetime, $\tau_i$	
	Expt.	Th-1	Th-2	Expt.	Th-1	Th-2a	Th-2b	Expt.	Th-1	Th-2a	Th-2b	Expt.	Th-1.
$0_1^+, 1 \quad 1_1^+, 0$	0.203	0.162	0.210						1.58	2.32	1.05		4.3 ps
$3_1^+, 0 \quad 1_1^+, 0$	0.444	0.394	0.980		84	2	9						0.56 ns
$1_2^+, 0 \quad 1_1^+, 0$	1.051	1.086	0.872	< 695	37	32	129	< 0.054	0.01	0.01	0.001	114(29) fs	287 fs
$0_1^+, 1$								0.78(24)	0.30	2.94	1.55		
$3_1^+, 0$				< 5329	30	56	224						
$2_1^+, 0 \quad 1_1^+, 0$	1.428	1.195	1.351	$b \times 3.2^a$	3.7	40	162	< 0.02	0.005	0.01	0.001	> 1.0 ps	2.6 ps
$0_1^+, 1$				$b \times 0.15$	0.21	0.3	0.3						
$3_1^+, 0$				$b \times 2.1$	54.6	12	48	< 0.005	0.002	0.007	0.001		
$1_2^+, 0$				$b \times 127.5$	127.5	2	7	< 0.05	0.0005	0.004	0.0003		
$4_1^+, 0 \quad 3_1^+, 0$	1.550	1.577	1.748	< 392	18.8	8	32	< 0.06	0.003	0.0	0.0	> 0.5 ps	10.2 ps
$2_1^+, 0$					88.5	28	112						
$3_2^+, 0 \quad 1_1^+, 0$	1.648	1.881	1.718	< 43	33.3	33	131					> 1.3 ps	1.9 ps
$3_1^+, 0$				< 20	4.8	2	7	< 0.006	0.0	0.0	0.0		
$1_2^+, 0$					109.4	4	18						
$2_1^+, 0$					35.2	2	9		0.002	0.002	0.0002		
$4_1^+, 0$					20.3	3	11		0.002	0.016	0.001		
$2_2^+, 1 \quad 1_1^+, 0$	1.653	1.782	1.580	< 60	0.4	0.6	0.6	< 0.011	0.0005	1.53	0.82	50(10) fs	30 fs
$0_1^+, 1$				122(47)	135.7	34	135						
$3_1^+, 0$				$2_{-2}^{+9}$	1.5	4	4	0.57(12)	1.0	4.32	2.3		
$1_2^+, 0$				27(22)	0.5	2	2	0.3(1)	0.29	0.23	0.15		
$2_1^+, 0$					1.12	0.2	0.2		0.31	1.02	0.4		
$4_1^+, 0$					0.28	0.4	0.4						
$3_2^+, 0$					0.42	0.7	0.7		0.065	0.068	0.04		
$5_1^+, 0 \quad 3_1^+, 0$	2.066	1.999	2.578	x	6.8	0.03	0.1						9.6 ps
$3_2^+, 0$				90(50)·x	90.7	23	92						
$4_1^+, 0$					47.8	6	25		0.003	0.0	0.0		
$4_2^+, 0 \quad 3_1^+, 0$	2.690(20)	2.532											
$4_3^+, 1 \quad 3_1^+, 0$	2.751	2.682	2.318		0.12	0.6	0.6	0.02(1)·y	0.01	0.004	0.005		70 fs
$3_2^+, 0$					0.25	2.2	2.2	y	0.16	1.30	0.75		
$2_1^+, 0$					0.03	0.01	0.01						
$2_2^+, 1$					76.8	23	87.8						
$5_1^+, 0$					0.0	0.4	0.4		0.017	0.001	0.001		
$4_1^+, 0$					0.14	0.2	0.2	1.2(4)·y	0.27	2.75	1.0		

<sup>a</sup> $b < 41$